Inversion-based correction of Double-Torsion (DT) subcritical crack growth tests for crack profile geometry

Seiji Nakagawa[a], Yida Zhang[b], Mehdi Eskandari-Ghadi[b], Donald W. Vasco[a]

[a]Energy Geosciences Division, EESA, Lawrence Berkeley National Laboratory, 1 Cyclotron Rd. MS74R316, Berkeley, 94720, CA, USA
[b]College of Engineering and Applied Science, University of Colorado, 1111 Engineering Dr, Boulder, 80309, CO, USA

Abstract

Because of its simplicity and the ability to produce a stable, slow-propagating crack, the Double-Torsion (DT) method has been used widely for investigating the critical and subcritical propagation of a slow-propagating tensile (mode-I) crack. However, to determine the complex relationship between the crack velocity v_c vs. the strain energy release rate $\mathcal{G}$ (or the stress intensity factor K) from laboratory measurements, several corrections must be made to account for the impact of sample and crack geometry. Particularly, DT test typically produces a crack with a curved edge profile instead of a straight line, causing the local v_c and $\mathcal{G}$ vary along the crack front. The experimentally measured v_c and $\mathcal{G}$ data merely reflect collective, averaged behavior of the crack. This makes inversion for the intrinsic, "true" crack growth kinetics necessary, based upon the knowledge of the crack geometry. Simple and effective correction methods have been proposed and validated for the slow, chemical-reaction-controlled part (Region I) of the $v_c - \mathcal{G}$ curve. However, reliable methods for the highly nonlinear, transport-dominated part (Region II) and its sudden transition to the dynamic propagation part (Region III) are still lacking. In this paper, we propose a method for determining the intrinsic v_c–$\mathcal{G}$ relationship cross all three Regions based upon DT test data, using a simple model function and its numerical inversion. The performance of this approach is examined and demonstrated using both synthetic and laboratory data for subcritical crack growth in soda lime glass.

Keywords: Subcritical crack growth, Double-Torsion test, Error corrections
PACS: 46.50.+a, 46.80.+j, 62.25.Mn
2000 MSC: 74A45, 74R10

1. Introduction

With increasing driving force, tensile (mode-I) crack propagation in brittle materials is known to exhibit complex kinetics [e.g. 1] (FIG.1). Initially, a crack grows slowly, but progressively faster, in a surface-reactive environment (Region I). This is usually followed by a stage where the velocity is relatively unchanged in spite of the increasing driving force, because the availability of the chemicals (including water) at the crack tip is limited by their transport along the crack (Region II). In the final stage, the stress state at the crack tip reaches the critical level at which the atomic bonds can break without the assistance of the chemical reactions (Region III). For many engineering problems, determining the long-term behavior in Region I, and the critical crack strength for rapid loading in Region III may be sufficient. However, crack propagation below the critical stress level—the *subcritical* crack growth, or, SCG—involves complex physico-chemical and mechanical interaction between crack surfaces which may be separated by only a few nanometers [2, 3], transport of gas and liquid within the nano-confined space near the crack tip [e.g. 4, 5, 6], and adsorption of fluid molecules along freshly created crack surfaces [7, 8]. These processes manifest themselves in the crack velocity vs. strain energy release rate ($v_c - \mathcal{G}$) relationship, both as the behavior within individual Regions and as their transitional characteristics such as threshold velocities and energy release rates. Thus, for investigating the rich physics underlying crack propagation, we are motivated to determine the entire SCG behavior accurately in the laboratory.

Because of its ability to produce a stable, slow-propagating crack, the Double-Torsion (DT) method has been used frequently for investigating the critical and subcritical propagation of a tensile crack. Its simple steps for determining the $v_c - \mathcal{G}$ relationship from an experiment on a plate sample, which is easy to prepare, made DT tests popular. However, over the years, it has been recognized that the original equations used for interpreting experimental data require several corrections for the errors introduced by a range of factors [e.g. 9, 10] related to the sample and crack geometries.

First, the effect of sample geometry (i.e. the ratios between the length L, width W, and the thickness h of a plate) can be significant and is particularly important. The original theory indicates that $\mathcal{G}$ is independent of the crack length a. However, experiments and numerical simulations have shown that

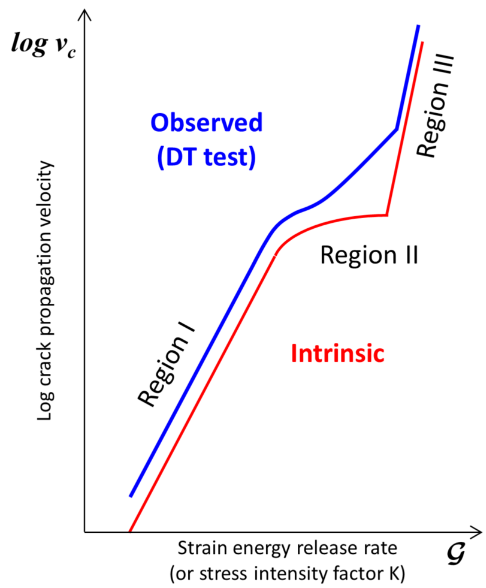

Figure 1: Typical characteristics seen in a crack propagation velocity v_c vs energy release rate $\mathcal{G}$ relationship for a tensile crack. Three regions with different propagation characteristics are identified. An experimental $v_c-\mathcal{G}$ relationship determined by a DT test (blue) tends to overestimate the propagation velocity, with a less pronounced "plateau" in Region II than the intrinsic relationship (red).

the actual $\mathcal{G}$ driving the crack is smaller than theory when a is small, and larger for as a approaches the length of the sample [e.g. 11]. As a result, experimentally obtained, uncorrected $v_c-\mathcal{G}$ relationships are also dependent on a and therefore an experiment involving multiple cycles of crack growth within a single sample produces different $v_c-\mathcal{G}$ curves. Ciccotti et al. [12] conducted a series of finite element simulations which examined the impact of L, W, h ratios, including the crack profile effect which will be discussed shortly, on the crack-length-dependent $v_c-\mathcal{G}$ curves. Their results indicate that, for samples with W/L less than 3, such effect becomes non-negligible. From a number of simulations, tables of correction factors were obtained, for both crack-length dependent parameter $B = B(a)$ and the energy release rate $\mathcal{G} = \mathcal{G}(a)$, which have been applied to correct the experimental results obtained using samples with smaller W/Ls [13].

A curved crack path also causes problems. Such a crack violates the original assumption of the theory—a straight crack—, resulting in increased

v_c for a given $\mathcal{G}$ as the crack length increases [e.g. 14]. To keep the crack path straight, DT tests often involve an added guiding groove. However, this can also lead to erroneous increases in v_c because of the locally introduced stress concentration around the groove. For this reason, experiments without a groove are preferred, with very careful alignment of the sample and the loading point to keep the crack path straight.

Lastly, the crack profile within a crack plane can introduce errors which more difficult experiments such as the Double Cantilever Beam (DCB) test [e.g. 15] are not affected by. This is because a DT test typically produces a crack with a curved edge profile instead of a simple, straight profile perpendicular to the primary plate surface. Therefore, v_c and $\mathcal{G}$ values reported from DT tests are the smeared outcome of the local velocities and the energy release rates which are varying along the crack front. This makes inversion for the intrinsic, "true" $v_c-\mathcal{G}$ relationship necessary, based upon the actual crack profile.

Several simple methods are available for correcting this crack profile effect. Evans [16] used a tilted straight profile, which approximates a curved crack profile, to estimate the actual v_c. Pollet & Burns [17] assumed a power-law relationship for the intrinsic $v_c-\mathcal{G}$, and obtained a simple method for correcting the experimental data, using a real crack profile. Although the Pollet-Burns method is an effective and robust correction technique for the slow propagation (Region I) of a crack, it does not account for the complex, highly nonlinear nature of a typically observed $v_c-\mathcal{G}$ relationship which has three distinct regions with different behavior (FIG.1). Particularly, in Region II with a distinct plateau structure, the Pollet-Burns method may results in large errors. Quantitative and reliable methods for determining a complex $v_c-\mathcal{G}$ curve are still not well developed to this day.

In this paper, we propose a method for determining the shape of a "typical" $v_c-\mathcal{G}$ relationship depicted in FIG.1, from a laboratory DT test. This method uses a simple model function with a series of control parameters which are inverted for numerically. In the following, we will first introduce the basic equations describing how the profile-based errors are introduced (Sec.2.2, 2.3). Subsequently, the conventional methods are reviewed (Sec. 2.4), and the new method is introduced (Sec. 2.5). Next, we will use synthetic data which simulate laboratory experiments, to examine the performance of this method (Secs.3.1, 3.2). The correction methods will also be used on our own laboratory DT test data for a soda-lime glass plate (Secs. 3.3 and 3.4). In both cases, the "correct" v_c–$\mathcal{G}$ is provided by the well-accepted Wiederhorn

[18]'s DCB experiment on soda-lime glass. The performance and validity of the proposed method will be discussed, and cautions and suggestions for its use will be provided (Sec. 3.5). Finally, the recommended procedure for applying the developed correction method is summarized (Sec. 4).

2. Crack-profile-error corrections

2.1. Basic experimental data interpretation

Because of its simplicity and the ability to produce a stable, slow-propagating crack, the Double-Torsion (DT) method has been used frequently for investigating the critical and subcritical propagation of a tensile crack. A typical DT test grows a single, straight crack along the center line of a thin rectangular plate which is supported at its four corners. The crack is driven by applying concentrated force on one plate edge to cause bending of the plate. For determining the $v_c-\mathcal{G}$ relationship, at minimum, only the displacement Δ and the force P at the loading point and several measurements of the crack length a during the experiment are necessary. The backbone of this simplicity is the robust, linear relationship between the loading-point compliance $C=\Delta/P$ and the crack length a [e.g. 19]

$$C = \frac{\Delta}{P} = Ba + D, \tag{1}$$

which is supported by both theory and experiments. Although the proportionality constant B can be determined theoretically from the sample properties and the loading configuration, it is more reliable to obtain both B and the system compliance D from an actual experiment. Using Eq.(1), the crack velocity is determined by

$$v_c = \frac{da}{dt} = \frac{1}{B}\frac{d}{dt}\left(\frac{\Delta}{P}\right) = \frac{1}{BP}\left(\frac{d\Delta}{dt} - \frac{\Delta}{P}\frac{dP}{dt}\right). \tag{2}$$

The energy release rate $\mathcal{G}$ is computed by [e.g. 19]

$$\mathcal{G} = \frac{P^2}{2h}\frac{dC}{da} = B\frac{P^2}{2h}, \tag{3}$$

where h is the thickness of the sample. Eq.(3) indicates that $\mathcal{G}$ is independent of the crack length. The "experimental" $v_c-\mathcal{G}$ relationship obtained from Eqs.(2) and (3) must be corrected for specific sample and crack geometries, in order to determine the true, intrinsic relationship.

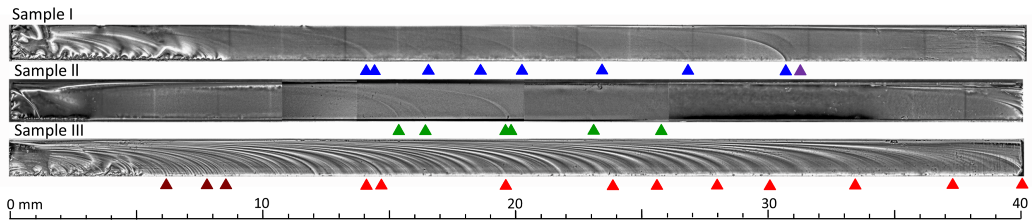

Figure 2: Optical crack surface images of three soda lime glass samples with different crack propagation velocities. The thickness of the samples is h=1.5 mm. Curved crack profiles were produced by applying abrupt changes in the propagation velocity (Samples I and II) and by instabilities of the produced crack plane caused by very fast crack propagation (Sample III). The triangles below the images are the leading edges of the profiles measured in FIG.3

2.2. Crack profiles generated by DT tests

Because a DT test induces a tensile crack by bending a plate, the resulting stress is not uniform across the thickness, which makes the crack profile asymmetric and often curved. This profile, defined by $x' = f(z)$ where x' is the distance along the length of the crack from the leading edge and z is the depth of the crack from the tensile side of the plate surface, respectively, may depend upon both crack length a and the apparent propagation velocity $\bar{v}_c$. However, it has been observed that, for a sample with the same geometry and material, the crack profile is not affected strongly by these factors [17]. This rather surprising property allows us to conduct error corrections based upon a single crack profile which may be observed during an experiment, or determined from fractographic images of a crack after the experiment.

In FIG.2, we present optical images of crack surfaces in soda lime glass samples from our DT tests (More epxerimental details are provided later in Sec.3.3). The samples were cracked under different loading rates, under similar relative air humidity of 30-40%. For each sample, abrupt changes in the loading rate resulted in a faint, crack-front profile which can be imaged by projecting light at an oblique angle onto the surface. For Sample I, the curved profiles were produced when rapid loading was applied after very slow propagation at $\bar{v}_c \approx 10^{-7} - 10^{-5}$ m/s. In contrast, in Sample II, the crack was first propagated at an intermediate rate of $\bar{v}_c \approx 10^{-4} - 10^{-3}$ m/s then was suddenly stopped by rapid unloading. These are approximate velocities determined from DT experiments via Eq.(2), without corrections for the crack front geometry. Reactivation of this arrested crack produced its profile. Lastly, for Sample III, the crack propagated in an uncontrollable fashion, at a velocity of $\bar{v}_c \geq 10^{-2}$ m/s. The resulting many, clearly visible crack profiles were possibly caused by the dynamic instability of a propagating crack front.

Selected crack profiles are compared for the three samples in FIG.3, fitted with the following continuous, monotonically increasing function which was found to fit very well to this data set:

$$\frac{x'}{h} = f(\zeta) = m_0 \left(-\frac{\pi}{2}\zeta + \tan\frac{\pi}{2}\zeta \right) + m_1\zeta + m_2\zeta^2 \tag{4}$$

where $\zeta = z/h$. Coefficients m_0, m_1 and m_2 are non-negative fitting parameters. Note that for the data shown in FIG.3, the crack profiles become vertical at the origin, allowing us to eliminate one of the fitting parameters (i.e., $m_1 = 0$). Although there are some differences (particularly, Sample II compared to Samples I and III), these profiles are remarkably similar, in spite of very different crack velocities and lengths. Note that the outlier I-9 for Sample I was produced when the crack was reactivated after it was fully unloaded for 3 days. The outliers for Sample III (I-1,2,3) are possibly affected by the interactions between the tail end of a crack with a notch at the head of the sample.

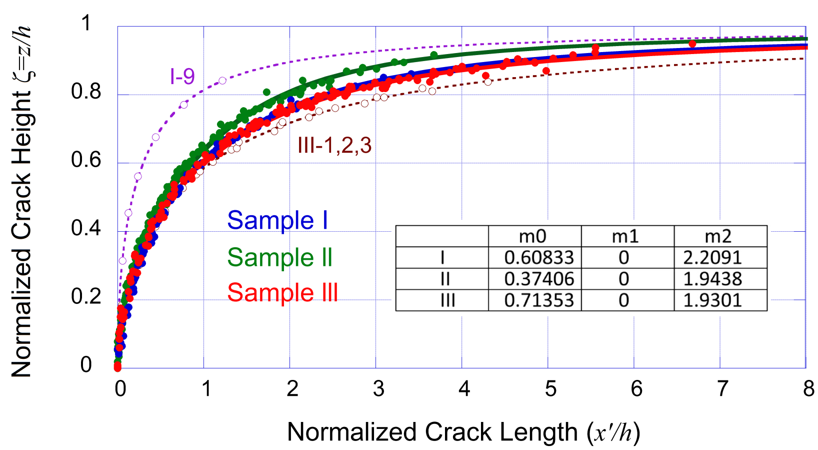

Figure 3: Crack profiles determined from photo images of the crack surfaces in FIG.2 . The crack length and the height are normalized by the thickness of the sample $h = 1.5$ mm.

2.3. Fundamental equations

As the experimental observations indicate, crack profiles from DT tests can be viewed approximately unchanged for different propagation velocities and lengths. An important consequence of this approximation is that a distribution of the local crack velocities, which is for the outward expansion of a crack perpendicular to a crack profile, is determined once the effective crack velocity $\bar{v}_c$ is provided by an experiment. Let the local crack velocity and strain energy release rate be v_c and $\mathcal{G}$, respectively. A crack front line segment ds to which these quantities are related forms an angle α against the sample surface (FIG.4). Experimentally observed α decreases monotonically from the leading edge of a DT crack. Considering that $dz = \sin\alpha ds$ where z is along the thickness of the sample, the energy balance between the local and the overall strain energy release rates for the crack propagating at an effective velocity $\bar{v}_c$ is stated as [e.g. 17]

$$\bar{\mathcal{G}}\left(\bar{v}_c\right)\ \bar{v}_c\ h = \int_s \mathcal{G}\left(v_c\right) v_c ds = \int_0^h \mathcal{G}\left[\bar{v}_c \sin\alpha\left(z\right)\right] \bar{v}_c dz \tag{5}$$

where h is the sample thickness. Therefore,

$$\bar{\mathcal{G}}(\bar{v}_c) = \int_0^1 \mathcal{G}\left[\bar{v}_c \sin\alpha(\zeta)\right] d\zeta \tag{6}$$

where $\zeta = z/h$.

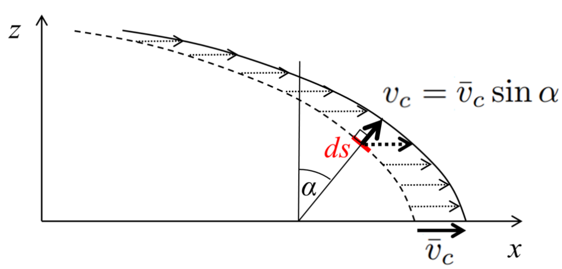

Figure 4: Relationship between the effective crack velocity $\bar{v}_c$ and the local crack velocity v_c. Translation of a crack profile in the x direction causes local outward expansion of the profile with an angle α, perpendicular to the local segment ds.

To help see what Eq.(6) implies, we provide a new form of this fundamental equation. By replacing the velocity and its reduction factor $\sin\alpha$ by their logarithmic counterparts (i.e. $\bar{u} = \ln\bar{v}_c$ and $u' = -\ln\sin\alpha$), Eq.(6)

can be written in a convolution form:

$$\bar{\mathcal{G}}(\bar{u}) = \int_{-\infty}^{+\infty} \mathcal{G}(\bar{u} - u\,')\Lambda(u\,')du\,' \tag{7}$$

$$= \int_{-\infty}^{+\infty} \Lambda(\bar{u} - u\,')\mathcal{G}(u\,')du\,'. \tag{8}$$

The function Λ is a dimensionless convolution kernel (or a Green's function) which can be derived from the substitution of the variable from ζ to u'. First, a crack profile $x/h = f(\zeta)$ (e.g., Eq.(4)) with monotonically changing $\alpha(\zeta)$ is determined by an experiment. Then, the function f, which computes α for a given ζ via $df/d\zeta = \cot\alpha$, is numerically reversed to find a function $\zeta = g(u')$ which computes ζs for given α $(= e^{-u'})$s. Using the relationship $d^2f/d^2\zeta = -(1/\sin\alpha^2)d\alpha/d\zeta$,

$$\Lambda(u') = \frac{d\zeta}{du'} = 1\bigg/\frac{du'}{d\zeta} = 1\bigg/\frac{du'}{d\alpha}\frac{d\alpha}{d\zeta} = \left.\frac{1 + (df/d\zeta)^2}{(df/d\zeta)(df^2/d\zeta^2)}\right|_{\zeta=g(u')}. \tag{9}$$

Note that Λ is defined 0 outside of the range $(0 \leq) - \ln\sin\alpha_{\mathrm{max}} \leq u\,' \leq - \ln\sin\alpha_{\mathrm{min}}$.

In FIG.5, several model crack profiles computed by Eq.(4) are presented, including experimental profiles for Samples I, II, and III. Corresponding Green functions are presented in FIG.6. A near-vertical crack front ($df/d\zeta \to 0$) and a near-straight profile ($d^2f/d\zeta^2 \to 0$) result in a sharp peak of Λ, which is also evident from Eq.(9). Also, an overall tilting of the profile increases $-\ln\sin\alpha_{\mathrm{max}}$, which shifts the function in the positive u' direction. For a curved profile, Λ becomes asymmetrically spread, causing distortions of $\bar{\mathcal{G}}$.

Our objective here is to determine the intrinsic function $\mathcal{G}(v_c)$ (or the v_c–$\mathcal{G}$ relationship) from an experimentally obtained function $\bar{\mathcal{G}}(\bar{v}_c)$ from a DT test. In principle, $\mathcal{G}$ can be determined by performing a deconvolution operation on Eq.(7), or by solving the integral equation Eq.(6) numerically by converting it into a linear system of equations. However, for the current problem, we found that this direct approach is highly sensitive to the noise (scatter) in the experimental data. Typically, the inverted model exhibits strong oscillation, and fails to capture the abrupt transition between the transport-dominated Region II and the crack behavior in vacuum in Region III (See Sec.3.2). Therefore, we use a more stable, indirect approach presented in Sec.2.5.

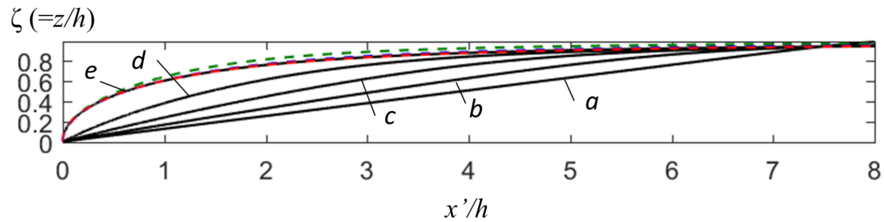

Figure 5: Crack profile models with a range of geometry, varying between a tilted and straight profile to more realistic, curved profiles. The models are computed by Eq.(4) using coefficients $m_0 = 0.71(1-\beta)$, $m_1 = 8\beta$, and $m_2 = 1.93(1-\beta)$ with β=0, 0.25, 0.5, 0.75, and 0.99 for the curves a through e respectively. The experimental profiles are also shown in broken lines. The length of the profiles is made finite ($8 \times h$) for easy comparison.

2.4. Conventional correction methods ("Shift" methods)

Before presenting a new method, in this section, we will first revisit the existing correction methods and examine them in light of the fundamental equations presented in Sec.2.3.

2.4.1. Evans' correction

Evans [16] noted that the experimentally measured crack propagation velocity $\bar{v}_c$ in a DT test must be corrected when the crack front is not perpendicular to the sample surface. Because the local, instantaneous crack growth direction is perpendicular to its leading edge, by approximating the crack profile as a straight line which intersects the sample surface at an angle α_0, the local, true crack velocity was determined by

$$v_c = \bar{v}_c \sin \alpha_0. \tag{10}$$

For brittle solids such as glass and ceramic, a reduction factor of $\sin \alpha_0 \approx 0.2$ was recommended.

Introducing Eq.(10) into Eq.(6) yields $\bar{\mathcal{G}}(\bar{v}_c) = \mathcal{G}(\bar{v}_c \sin \alpha_0)$. Substituting the variables as before,

$$\mathcal{G}(\bar{u}) = \bar{\mathcal{G}}(\bar{u} - \ln \sin \alpha_0). \tag{11}$$

Comparing this result to Eq.(7), we find

$$\Lambda(u') = \delta(u' + \ln \sin \alpha_0). \tag{12}$$

In FIGs 5 and 6, this result approximately corresponds to the crack model a which has a profile close to a straight line.

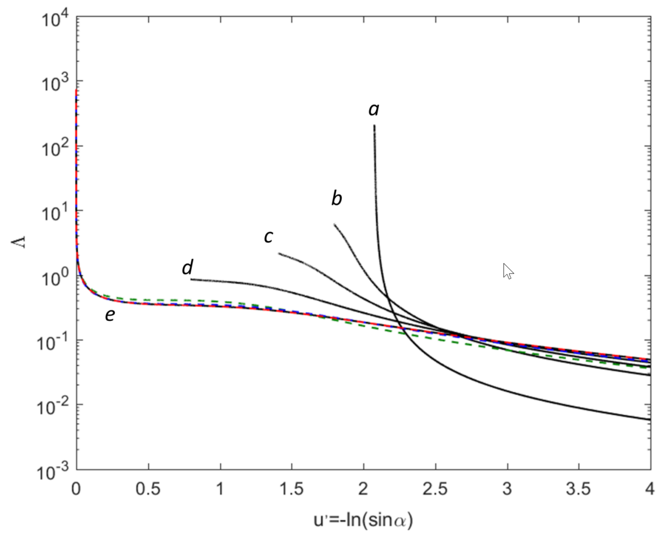

Figure 6: Green functions Λ for the crack profiles in FIG.5. These functions are assymmetric, and approach a Dirac delta function for straight profiles. Also, the overall tilting of the profile offsets the peak of the related Λ in the positive direction.

2.4.2. Pollet-Burns correction

Because using a straight line to approximate a curved profile can introduce large errors in the estimated local crack velocities, it is desirable to take into account the real crack profile in the correction.

Pollet & Burns [17] noticed that when the $v_c - \mathcal{G}$ relationship can be modeled by a power law

$$v_c = C\left(\frac{\mathcal{G}-\mathcal{G}_0}{\mathcal{G}_0}\right)^n, \text{ i.e., } \mathcal{G} = \mathcal{G}_0\left[1+\left(\frac{v_c}{C}\right)^{\frac{1}{n}}\right], \tag{13}$$

introducing $v_c = \bar{v}_c \sin\alpha$ into Eq.(6) results in

$$\bar{\mathcal{G}}(\bar{v}_c) = \mathcal{G}\left(\bar{v}_c\phi\right), \text{ or, } \mathcal{G}\left(\bar{v}_c\right) = \bar{\mathcal{G}}(\bar{v}_c/\phi) \tag{14}$$

where

$$\phi \equiv \left[\int_0^1 \left(\sin\alpha(\zeta)\right)^{\frac{1}{n}} d\zeta\right]^n. \tag{15}$$

By replacing the variables by their logarithimic counterparts as $\bar{v}_c \to \bar{u} \equiv \ln\bar{v}_c$, $\bar{v}_c/\phi \to \bar{u} - \ln\phi$, we have

$$\mathcal{G}(\bar{u}) = \bar{\mathcal{G}}\left(\bar{u} - \ln\phi\right). \tag{16}$$

For ns larger than 4-5 (which is usually the case), ϕ is nearly constant (FIG.7). Similar to Eq.(11), Eq.(16) indicates that the intrinsic function $\mathcal{G}(v_c)$ can be obtained by simple "shifting" (reducing) of an experimentally obtained function $\bar{\mathcal{G}}(\bar{v}_c)$ by $-\ln\phi(>0)$ along the logarithmically scaled velocity axis. However, the Green function Λ is determined by Eq.(9) from an experimental crack profile, and generally is not a Delta function.

As a new result, we also found that the Pollet and Burns' approach can be used with an exponential (or Arrhenius) $v_c-\mathcal{G}$ relationship

$$v_c = v_0 \exp k\left(\frac{\mathcal{G}-\mathcal{G}_0}{\mathcal{G}_0}\right), \text{ i.e., } \mathcal{G} = \mathcal{G}_0\left[1+\frac{1}{k}\ln\left(\frac{v_c}{v_0}\right)\right], \tag{17}$$

which leads to the same result as Eq.(15) but with

$$\phi \equiv \exp\int_0^1 \ln\sin\alpha(\zeta)d\zeta \tag{18}$$

Note that this equation does not contain the exponent factor k. Also, Eq.(15) can be shown to converge to Eq.18 when $n\to\infty$. (FIG.7).

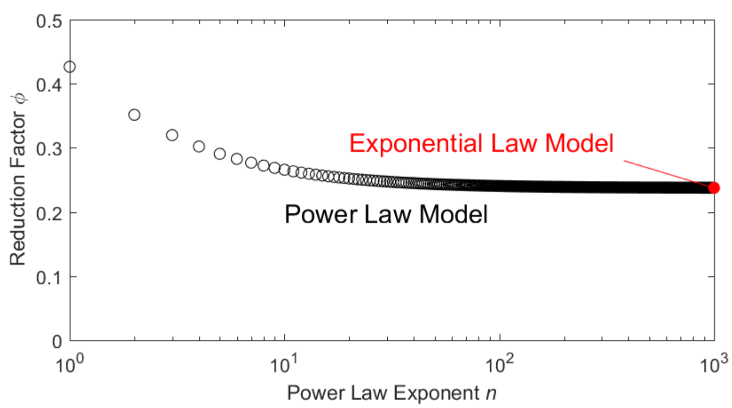

Figure 7: Reduction factor ϕ for a range of power law exponent n. The value for the exponential law model is also shown (solid red circle). For large ns, ϕ is nearly constant, and converges to the exponential law model.

2.5. Parameterized inversion via fitting of a specific $v_c-\mathcal{G}$ model

As seen in Sec.2.4, existing correction methods make an assumption of either a highly idealized crack profile (Evans' correction) or a simplified (power-law [Pollet-Burns] or exponential-law) v_c–$\mathcal{G}$ relationship. However, an actual, curved crack profile and complex $v_c-\mathcal{G}$ relationship can lead to large errors. In fact, many experimental data on brittle materials show three distinct regions in their $v_c-\mathcal{G}$ relationships, as depicted in FIG.1 (refs): Region I can be described routinely by a power or exponential law; which gradually transitions to Region II where v_c is much less sensitive to $\mathcal{G}$; and finally, in Region III, the behavior follows another power or exponential law with a much steeper slope than Region I. The transition from II to III is usually abrupt, often resulting in a sharp kink in the curve. These characteristics were also confirmed recently by first-principle-based simulations conducted by the authors [20].

To determine the complex shape of the intrinsic $v_c-\mathcal{G}$ curve from a DT test while taking into account the typical curved crack profile, we propose an indirect inversion method based upon a simple but flexible analytical $v_c-\mathcal{G}$ model.

2.5.1. Parameterized model functions

The model is parameterized by a limited number of control variables, considering the constraints provided by the aforementioned characteristics of experimentally observed $v_c-\mathcal{G}$ curves:

$$\mathcal{G}\left(v_c\right)=\begin{cases}\displaystyle\sum_{n=0}^{N_{\mathrm{I}}} c_n^{\mathrm{I}}\xi^n, & \xi\leq 0 \quad \text{(Region I)}\\ c_0^{\mathrm{II}}+c_1^{\mathrm{II}}\xi+c_2^{\mathrm{II}}\left(1-\sqrt{1-\xi^2}\right), & \\ & 0<\xi\leq 1 \quad \text{(Region II)}\\ \displaystyle\sum_{n=0}^{N_{\mathrm{III}}} c_n^{\mathrm{III}}\eta^n, & \eta\geq 0 \quad \text{(Region III).}\end{cases} \tag{19}$$

In Eq.(19), dimensionless local coordinates ξ and η are used, which are defined by

$$\begin{aligned}\xi&=(\log v_c-\log v_{cT})/(\log v_{cD}-\log v_{cT}),\\ \eta&=(\log v_c-\log v_{cD})/(\log v_{cD}-\log v_{cT}),\end{aligned} \tag{20}$$

In Eq.(20), v_c is the primary variable, because we will use Eq.(6) with $v_c=\bar{v}_c\sin\alpha$ to solve for the model. v_{cT} and v_{cD} are the transition crack velocities at the Regions I-II and Regions II-III boundaries, respectively. Requiring C_0

and C_1 continuity of the functions at $v_c = v_{cT}$, and C_0 continuity at $v_c = v_{cD}$, we have

$$
\begin{aligned}
c_0^{\mathrm{II}} &= c_0^{\mathrm{I}}, \\
c_1^{\mathrm{II}} &= c_1^{\mathrm{I}}, \\
c_2^{\mathrm{II}} &= c_0^{\mathrm{III}} - c_0^{\mathrm{I}} - c_1^{\mathrm{I}}.
\end{aligned} \tag{21}
$$

Therefore, the coefficients c_0^{II}, c_1^{II}, and c_2^{II} in Eq.(19) are not independent variables. In Eq.(19), the functions for Regions I and III are low-order polynomials, and we choose $N_{\mathrm{I}} = 1$ or 2 and $N_{\mathrm{III}} = 0$ or 1, considering the quality of typically obtained laboratory data found in the literature (e.g., Wiederhorn, 1967). The equation for Region II is the key part of this model, which accounts for the characteristic plateau (near-constant v_cs) over a range of $\mathcal{G}$s. The difference $v_{cD} - v_{cT}$ controls the sharpness of the transition from Region I to Region II.

2.5.2. Liner inversion

Introducing Eqs.(19) into Eq.(6) results in a series of linear system of equations for the energy release rates predicted by the model, for apparent (experimentally observed) crack velocities $\bar{v}_c^{(i)}$ where $i = 1, 2, .. N_{obs}$.

$$
\mathcal{G}_{pre}(\bar{v}_c^{(i)}) = \int_0^1 \mathcal{G}\left[\bar{v}_c^{(i)} \sin\alpha(\zeta)\right] d\zeta = \boldsymbol{A}\boldsymbol{x} \tag{22}
$$

where $\boldsymbol{A}$ is the coefficient matrix which is computed using Eq.(19), and $\boldsymbol{x}$ is a vector containing the unknown coefficients c_n^{I} and c_n^{III}. For $N_{\mathrm{I}} = 2$ and

$N_{\mathrm{III}} = 1$,

$$
\begin{aligned}
\boldsymbol{A} &= \begin{bmatrix} A^{\mathrm{I}}_{10} & A^{\mathrm{I}}_{11} & A^{\mathrm{I}}_{12} & A^{\mathrm{III}}_{10} & A^{\mathrm{III}}_{11} \\ \vdots & \vdots & \vdots & \vdots & \vdots \\ A^{\mathrm{I}}_{N_{obs}0} & A^{\mathrm{I}}_{N_{obs}1} & A^{\mathrm{I}}_{N_{obs}2} & A^{\mathrm{III}}_{N_{obs}0} & A^{\mathrm{III}}_{N_{obs}1} \end{bmatrix}, \\
A^{\mathrm{I}}_{in} &= \int_0^1 \left[\begin{array}{c} W^{\mathrm{I}}(\xi)\xi^n + W^{\mathrm{II}}(\xi)\xi^n \\ -W^{\mathrm{II}}(\xi)(1-\sqrt{1-\xi^2}) \end{array} \right] d\zeta,\ (n=0,\ 1) \\
A^{\mathrm{I}}_{i2} &= \int_0^1 W^{\mathrm{I}}(\xi)\xi^2 d\zeta, \\
A^{\mathrm{III}}_{i0} &= \int_0^1 \left[\ W^{\mathrm{III}}(\eta) + W^{\mathrm{II}}(\xi)(1-\sqrt{1-\xi^2})\ \right] d\zeta, \\
A^{\mathrm{III}}_{i1} &= \int_0^1 W^{\mathrm{III}}(\eta)\eta d\zeta, \\
\boldsymbol{x} &= \left[\ c^{\mathrm{I}}_0 \quad c^{\mathrm{I}}_1 \quad c^{\mathrm{I}}_2 \quad c^{\mathrm{III}}_0 \quad c^{\mathrm{III}}_1.\ \right]^T.
\end{aligned}
\tag{23}
$$

where ξ and η are provided by Eq.(20) with $v_c = \bar{v}_c^{(i)} \sin\alpha(\zeta)$ for each row (or data point) i. The functions $W^{\mathrm{I}}(\xi)$, $W^{\mathrm{II}}(\xi)$, and $W^{\mathrm{III}}(\eta)$ are the weight functions which are 1 within the related Regions (I, II, and III, respectively), and 0 elsewhere. By comparing these predictions to the experimentally observed data $\boldsymbol{b} = \left[\bar{\mathcal{G}}_{obs}(\bar{v}_c^{(i)})\right]$, we obtain the residual vector

$$
\begin{aligned}
\boldsymbol{r} &= \left[\bar{\mathcal{G}}_{obs}(\bar{v}_c^{(i)})\right] - \left[\mathcal{G}_{pre}(\bar{v}_c^{(i)})\right], \\
&= \boldsymbol{b} - \boldsymbol{A}\boldsymbol{x}
\end{aligned}
\tag{24}
$$

The least-square solution for the unknown coefficients which minimizes the L_2 norm of $\boldsymbol{r}$ is, assuming we have equal or more data points than the number of unknown coefficients (i.e. an over-determined problem),

$$
\boldsymbol{x} = \left(\boldsymbol{A}^T\boldsymbol{A}\right)^{-1}\boldsymbol{A}^T\boldsymbol{b}. \tag{25}
$$

Note that the data can be weighted by a diagonal data weight matrix $\boldsymbol{W}_D$ as $\boldsymbol{W}_D\boldsymbol{b}$, for the number of the available data in each Region and their relative importance (or quality). In this case, the least-square solution is given by

$$
\boldsymbol{x} = \left(\boldsymbol{A}^T\boldsymbol{W}_D^2\boldsymbol{A}\right)^{-1}\boldsymbol{A}^T\boldsymbol{W}_D^2\boldsymbol{b}. \tag{26}
$$

2.5.3. Nonlinear inversion

The minimized misfit $\boldsymbol{r} = \boldsymbol{r}_{\min}$ between the prediction and the data in the linear problem is a nonlinear function of v_{cT} and v_{cD} which are treated as constants in the linear inversion. To find the best-fit model which is defined by both linear parameters c_n^{I} and c_n^{III} and the nonlinear parameters v_{cT} and v_{cD}, we solve this nonlinear optimization problem by iteratively minimizing the L_1 or L_2 norm of the residual vector $\boldsymbol{r}_{\min}$. Because we need to solve for only two unknowns v_{cT} and v_{cD}, in this study, we use the Nelder-Mead simplex method [21] which is effective for low-dimension problems. The necessary inequality constrains

$$0 < v_{cT} < v_{cD}. \tag{27}$$

are applied by the penalty method.

Initial values for v_{cT} and v_{cD} are needed to start this simplex inversion. In laboratory data, an approximate v_{cT} can be found by identifying the inflection point immediately following the shoulder of an experimental $\bar{v}_c - \bar{\mathcal{G}}$ curve, and reducing that by the peak shift of the Green function computed by Eq.(9). In FIG.8, predicted experimental $\bar{v}_c - \bar{\mathcal{G}}$ curves are shown which are computed for an assumed, intrinsic v_c–$\mathcal{G}$ relationship (bold red curve), using the crack profiles in FIG.5 and Eq.(6). Note that the offsets of the inflection-point velocities u' from v_{cD} are converted from base-10 to base-e (natural) logarithm, so that they can be compared to the offsets of the Green function peak in FIG.6. Also note that, as seen from Case e in FIG.8, for a crack profile with a near-vertical leading edge such as FIG.3, the inflection point directly provides v_{cD}.

In contrast to v_{cD}, the gradual change between Regions I and II makes it difficult to identify v_{cT}. Currently, we arbitrarily choose v_{cT} given by $\approx 0.3 \times v_{cD}$ as the initial guess.

2.5.4. Constraining Region I and III behavior

The intrinsic $v_c - \mathcal{G}$ relationship for Region I can be determined by using the shift methods described in Sec.2.4. This is because a power law is applicable for chemically controlled, slow crack propagation. The shift method may also be applied to the fast crack propagation in Region III. However, when the Green function Eq.(9) has a long "tail", because of the smearing effect from Region II, the intrinsic relationship may agree with the shift method only asymptotically. Therefore, if good quality laboratory data are available

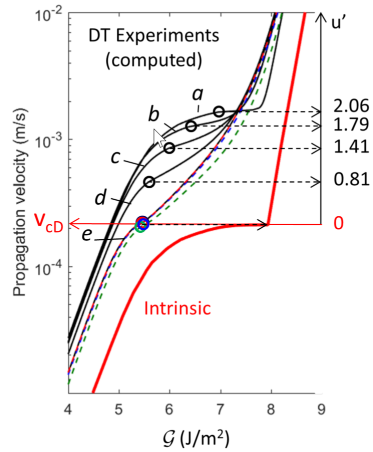

Figure 8: Identification of an approximate Region II to Region III transition velocity v_{cD} from an experimental $\bar{v}_c - \bar{\mathcal{G}}$ curve and a crack profile. Here, the experimental curves are computed from an assumed intrinsic $v_c - \mathcal{G}$ relationship and the crack profiles a-e in FIG.5. The offset $u' = -\ln(v_{cD} - v_{cI})$ between the inflection point velocities v_{cI} of the experimental curves and v_{cD} correspond to the peak shift of the Green function given in FIG.6.

for a broad range of crack velocities, the model functions for one (typically Region I) or both of these regions can be determined by simply fitting polynomials in Eq.(19) to the shifted data, without using the linear inversion. When both c_n^{I} and c_n^{III} are determined this way, the remaining unknowns are only the transition velocities v_{cT} and v_{cD}. Additionally, if the inflection point of an experimental $\bar{v}_c - \bar{\mathcal{G}}$ curve can be clearly identified, v_{cD} can be simply computed using the peak offset of the Green function, further reducing the number of unknowns, as demonstrated by FIG.8. Note that the coefficients c_n^{I} and c_n^{III} still need to be updated at each step of the nonlinear inversion, because they depend upon v_{cT} and v_{cD}.

3. Examples and discussion

In this section, we will examine the performance of the proposed methods by using both simulated (synthetic) and laboratory-measured DT test data on soda-lime glass.

3.1. Synthetic data

First, we examine the performance of the proposed methods by using simulated experimental data. As the "true", intrinsic $v_c - \mathcal{G}$ relationship, we choose to use the Wiederhorn [18]'s results for soda lime glass, obtained via DCB tests [e.g. 15]. This is because, unlike a DT test, a DCB test produces a straight crack profile and does not require the the crack-profile-related corrections. Also, we use the relative humidity=100% case from the experiment, because it shows well-defined three Regions in its $v_c - \mathcal{G}_\mathrm{I}$ curve, and the accompanying plot of scattered data provides us with estimates about the magnitude of experimental errors. Note that for the remainder of Section 3, we will present the Widerhorn [18]'s results as a $v_c - \mathcal{G}$ curve instead of a $v_c - K_I$ relationship, assuming soda lime glass's Young's modulus E to be 72 GPa. Because a propagating crack in DCB tests is under an approximately plain stress state, $\mathcal{G}$ and K_I are related via $\mathcal{G} = K_I^2/E$.

For simulating experiments, we use Eq.(6) to compute 30 data points in the range of $10^{-8} < \bar{v}_c < 10^{-2}$ m/s. Additionally, we add 0%, 2%, 5%, and 10% (standard deviation) of Gaussian noise to the computed logarithmic crack velocity, to examine the impact of experimental errors on the inversion. The assumed crack profile is that of Sample II, which is given in FIG.3.

3.2. Inversion using synthetic data

The results of the inversion are shown in FIG.9. In the figure, the black line is the "true" response (i.e. "correct" solution). The blue closed circles are computed by applying Eq.(6) to the true response, simulating what would be observed experimentally by a DT test. The open red circles are the $v_c - K_\mathrm{I}$ relationship which was obtained by applying the shift method to the simulated DT data. We assumed the Arrhenius model and used Eq.(18) to compute the shift parameter. Note that no *a priori* knowledge of the characteristics of the true response is needed by the shift method. It can be seen that the errors are large for the Region II part of the solutions. The corrected v_c–K_I relationships which were obtained by the proposed inversion method using a prescribed model are shown in red curves. Finally, the best-fit experimental responses predicted by the inverted models are shown in blue curves, which can be compared to the original simulated data (blue closed circles) for fit errors. For this example, both linear and nonlinear inversion in 2.5 were conducted simultaneously.

The results indicate that new inversion method works well for a moderate levels of noise. Although increases in the noise makes transition between Regions I and II less accurate, overall, the plateau in the $v_c - \mathcal{G}$ is captured more accurately, compared to the shift method. For a large noise level ($\sigma = 5 - 10\%$), the inversion becomes less accurate, and the shift method may

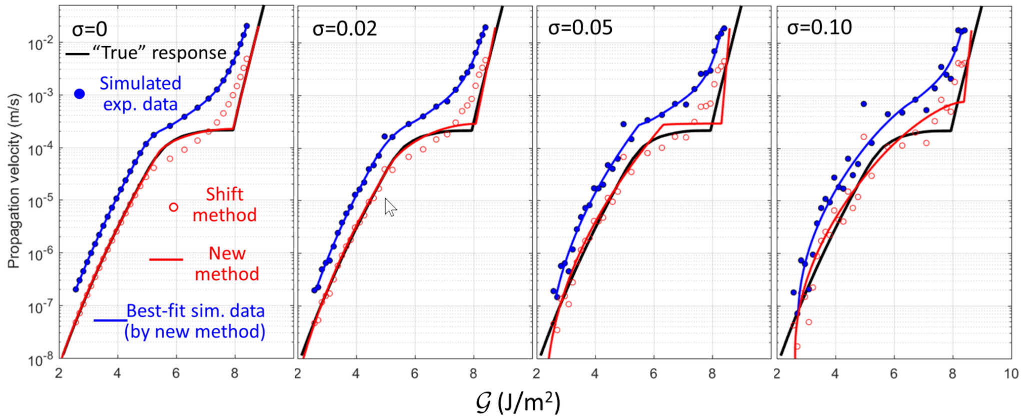

Figure 9: The effect of data noise (scatter) on inversion. A model (black curve) was used to generate simulated experimental data (closed blue circles) with a range of noise levels. The parameterized inversion was conducted (red curves) and compared to the original model, and also to the result of the shift method (open red circles). The shift method results in large errors in Region II, but in good agreement for Region I and for the high-velocity end of Region III. The parameterized model performs well even when a moderate level of noise ($\sigma = 0.05$) is present in the experimental data.

provide a more robust answer. This example also demonstrates that the shift method provides accurate results in Region I, and also asymptotically for the high-velocity part of the curve in Region III. As mentioned in 2.5.4, this can be used to improve the robustness of the inversion.

For comparison, we also present the results of direct inversion based upon discretization of Eq.(6) with an unknown $\mathcal{G}$ vector. A generalized inverse of the coefficient matrix is computed by the singular-value decomposition (SVD) method [e.g. 22]. A noise-free case ($\sigma = 0$) and 2% noise case ($\sigma = 0.02$) are shown in FIG.10. The direct inversion performs reasonably well for the zero-noise case, capturing the abrupt changes around Region II part of the model. However, introduction of small noise results in strong oscillation of the solution, indicating this inversion is not stable.

3.3. Laboratory data

Next, we use our own DT test results for soda-lime glass samples. These samples are rectangular plates with length (L) $\times$ width (W) $\times$ thickness (h) $= 40$ mm $\times$ 20 mm $\times$ 1.5 mm. In order to prevent uncontrollable catastrophic crack propagation, a short (1.5 mm) precrack was introduced by a thermal

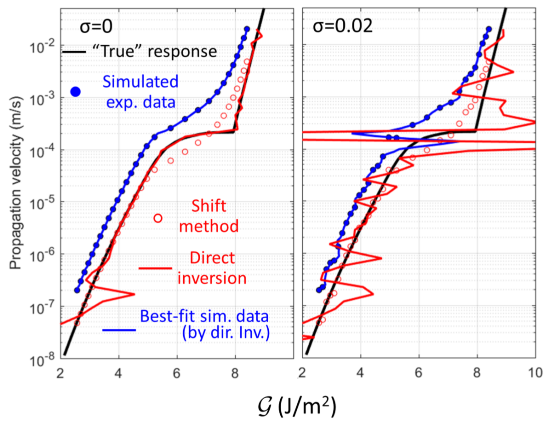

Figure 10: Results of the direct inversion by solving a discrete linear system of equations via SVD. When there is no noise (σ=0), except for the low velocity end, the intrinsic behavior can be inverted for accurately. However, low-level noise (σ=0.02) results in strong oscillations in the result.

shock. One of the samples (case 1) was measured for the crack profiles, which were presented as Sample II in FIG.s 2 and 3.

The rectangular sample was supported by four stainless steel ball bearings with a diameter d=1.6 mm it its corners, and a pair of concentrated force was applied by the same type of ball bearings (1.6 mm apart) at the edge of the sample, straddling the precrack. During the experiment, the sample was initially loaded at a displacement rate of 1 μm/s using a piezoelectric linear actuator (Polytec, PICMAwalk N331.13). Once the crack started to grow, the displacement was held constant at multiple force intervals and the relaxation of the loading-point force were monitored using a load cell (Transducer techniques, MDB-10), to determine the time-dependent compliance changes given in Eq.(1). Concurrently, the crack length was measured using an optical microscope, and correlated with the compliance.

Once the crack velocity and the strain energy release rate were computed using Eqs.(2) and (3), the experimental energy release rate $\bar{\mathcal{G}}_{exp}$ was corrected for the crack-length effect for the current sample geometry. For this, we used the following experimentally determined relationship, instead of using the published data based upon finite element models [12]

$$\bar{\mathcal{G}}(a) = \bar{\mathcal{G}}(a)_{exp} \times \begin{cases} e^{-s^2/49} & (a \leq a_c) \\ e^{s^2/32} & (a \geq a_c). \end{cases} \tag{28}$$

where

$$s = L(a - a_c)/a_c^2, \;\; a_c = (L - 0.5d)/2.$$

This equation was derived from multiple, repeated crack growth measurements in soda lime glass for a range of crack lengths, so that the experimental $\bar{v}_c - \bar{\mathcal{G}}$ curves converged to a single curve for crack lengths $a \approx a_c$.

3.4. Inversion using laboratory data

The results for two experiments are shown in FIG.11. The dark (Case 1) and light (Case 2) filled blue circles are the experimental data after the sample geometry correction by Eq.(28). First, for comparison, results of the conventional shift method are presented in open red (Case 1) and orange (Case 2) circles. Next, the results of unconstrained (i.e. both linear and nonlinear inversion were conducted simultaneously) inversion are shown in thick curves of the corresponding colors. The DT test responses predicted by these inverted models are also presented, showing excellent agreement with the experiment.

The inverted results are then compared to the Wiederhorn's experimental data in FIG.12. Our experiments were conducted under a relative humidity (RH) of 32 to 34% at $22°C$. The inverted results are generally in good agreement with the published data, slightly above the RH=30% curve.

From FIGs.11 and 12, the new inversion method works well for Regions I and II, capturing the gradual transition between the Regions and the plateau behavior. Although the Wiederhorn[18] lacks relevant data for Region III, our inversions seem rather unreliable for this part. This is probably because the rapid relaxation of the test system introduced errors in our measurements, as indicated by the large differences in the two sets of data for Region III, compared to Regions I and II.

When the availability of data in Region III is severely limited, additional constraints to the model can be applied. For example, the slope in the $v_c - \mathcal{G}$ curve can be assumed, or simply given by a constant value $\mathcal{G} = \mathcal{G}_c$ (critical energy release rate). Although this does not help determining the behavior of high-velocity crack propagation in Region III, it will still improve the accuracy of the inverted true crack behavior in and around Region II.

3.5. Potential improvements and future directions

Further extensions and improvements of the proposed method can be pursued along the following directions.

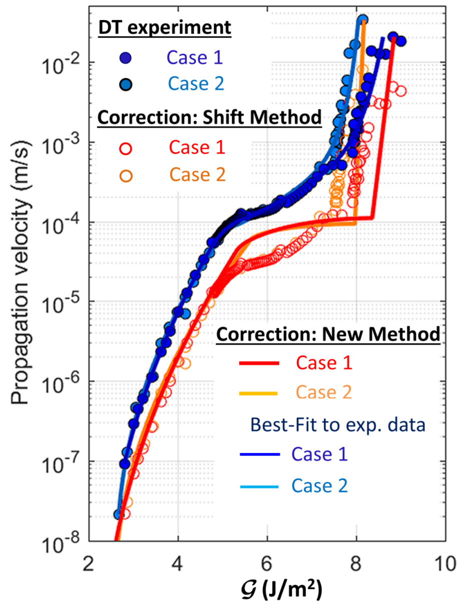

Figure 11: Inversion of the intrinsic response from our DT experiment on a soda lime glass sample (solid blue circles). Inversion results for both cases with and without constraining the Regions I and II parts via a shift method (open red circles) are shown (red and orange curves, respectively). Predictions by the inverted models (dark and light blue curves, respectively) are also shown for comparison with the experimental data.

First, the inversion relies upon a laboratory-observation-based assumption that for the same material and environmental conditions, the DT crack profile is largely unchanged for different crack lengths and propagation velocities. This allows us to estimate quantitatively how the true, local crack propagation velocity varies along a crack front, from a single, measured effective propagation velocity. Currently, a theoretical explanation of this interesting and very useful property is lacking. For this reason, when a DT experiment is performed using very different testing conditions and materials, the crack profile has to be measured for the specific sample used in the test.

Also, our inversion method uses a specific function to represent the crack behavior for Region II. The proposed simple function fits very well the soda-lime glass data investigated in the current study. Currently, however, there is no theoretical backing and guarantee that the prescribed shape of the function can accurately represent the intrinsic $v_c - \mathcal{G}$ behavior of any other materials under different test conditions. Further validation of the proposed

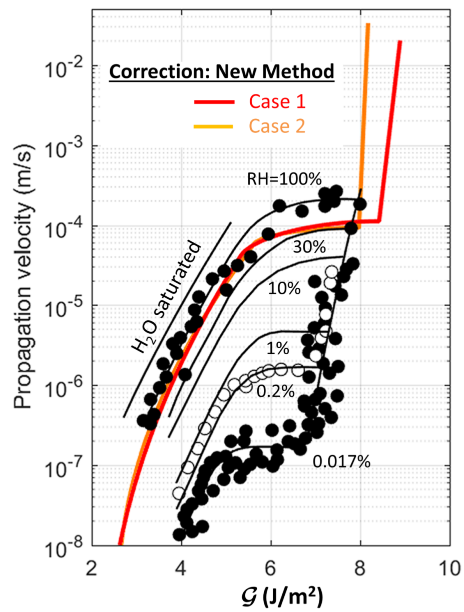

Figure 12: Comparison of the inverted results in FIG.11 with Wiederhorn [18]'s experimental data. The inversion of our own laboratory data with RH=32-34% generally shows good agreement with the Wiederhorn's RH=30% data.

function, and development of more sophisticated functions based upon the underlying physical processes may be necessary.

Lastly, we point out that many published DT test results are not corrected for the crack profile effect discussed in this paper, which can leads to (1) overly sensitive crack velocity changes to the applied force increases in Region II, (2) a gradual Region II to III transition, and (3) underestimation of the critical energy release rate (or stress intensity factor). The proposed inversion method would improve the accuracy of the v_c–$\mathcal{G}$ relationship determined by DT tests, which can help provide experimental data elucidating the complex kinetics involved in subcritical crack propagation, particularly within and around Region II.

4. Conclusions

Although the Double-Torsion (DT) test can provide the relationship between both critical and subcritically applied driving force and the crack propagation velocity, the obtained data need to be corrected for a variety of geometric effects to obtain the true crack growth kinetics. We propose a new method for correcting for the crack-profile-induced overestimation errors in crack propagation velocities, using a prescribed model between the crack velocity and the energy release rate. The proposed method is validated by the published data and our own experimental data for soda lime glass samples under ambient conditions.

Following the examples provided in Sec.3, we suggest the following procedure to determine the intrinsic v_c–$\mathcal{G}$ relationship based upon DT tests (see FIG.13):

1. Collect low-noise data which exhibit both Regions I and III parts in the experimental $\bar{v}_c$–$\bar{\mathcal{G}}$ curve, and also obtain a crack profile from the DT test
2. Conduct the standard DT data processing, including necessary corrections for the sample geometry and crack length effect.
3. Compute a shift parameter ϕ from the crack profile. Using ϕ, determine the low-velocity behavior in Region I, and high-velocity asymptotic behavior in Region III.
4. Select from the $\bar{v}_c - \bar{\mathcal{G}}$ curve a sharp change in the slope. From the crack-profile Green function, determine the peak velocity offset. From these, determine the initial estimate for the Region II-III transition velocity v_{cD}, then Region I-II transition velocity v_{cT}.
5. Perform the iterative, combined linear-nonlinear inversion to determine optimal polynomial coefficients, v_{cD}, and v_{cT}.
6. During the inversion, Region I and III behavior and v_{cD} can be constrained to improve the robustness of the inversion, depending on the quality and availability of the experimental data.
7. Check the quality of the fit by comparing the experimental data and the predicted response by the inverted, v_c–$\mathcal{G}$ model. Confirm that the Region I behavior agrees with the shift method in Step 3, and also that the Region III behavior asymptotically matches the shift method.

Note that because the knowledge of the crack front profile is indispensable for using this method, the crack profile data needs to be obtained in addition to the loading-point displacement and reaction force, and the crack length from a DT test.

The proposed method improves the validity of the v_c–$\mathcal{G}$ relationships determined by DT tests to the Region II and III parts. This allows quantitative evaluation of the crack behavior controlled by—or limited by—transport of fluid and dissolved chemicals near the crack tip. Using this method, results of DT tests can be used to investigate the impact of humidity and aqueous fluid chemistry on subcritical crack growth under these still not well-understood crack propagation regimes in brittle solids.

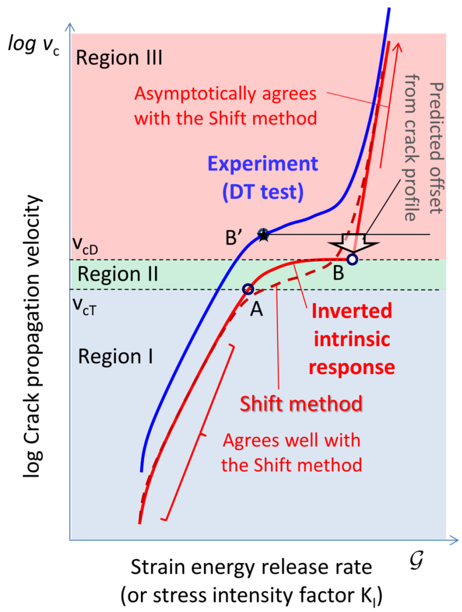

Figure 13: A summary of the proposed inversion method. Experimental, overestimated v_c–$\mathcal{G}$ curve (blue) is corrected first by the shift method (red broken curve), which is used to determine the behavior for Region I. Subsequently, the Regions II and III parts of the prescribed nonlinear model (solid red line), where the shift method can be inaccurate, are determined via linear inversion for the fitted polynomial coefficients, and nonlinear inversion for transition velocities v_{cT} and v_{cD}. The initial estimate of v_{cT} is determined from an inflection point of the experimental curve.

Acknowledgement

This research was supported by the Office of Science, Office of Basic Energy Sciences, Division of Chemical Sciences of the U.S. Department of Energy, under Contract No. DE-AC02-05CH11231.

References

[1] B. K. Atkinson, Subcritical crack growth in geological materials, Journal of Geophysical Research: Solid Earth 89 (B6) (1984) 4077–4114.

[2] J. Israelachvili, Forces between surfaces in liquids, Advances in Colloid and Interface Science 16 (1) (1982) 31–47.

[3] J. Dziadkowiec, S. Javadi, J. E. Bratvold, O. Nilsen, A. Røyne, Surface forces apparatus measurements of interactions between rough and reactive calcite surfaces, Langmuir 34 (25) (2018) 7248–7263.

[4] J.-G. Choi, D. Do, H. Do, Surface diffusion of adsorbed molecules in porous media: Monolayer, multilayer, and capillary condensation regimes, Industrial & engineering chemistry research 40 (19) (2001) 4005–4031.

[5] A. Cihan, T. K. Tokunaga, J. T. Birkholzer, Adsorption and capillary condensation-induced imbibition in nanoporous media, Langmuir 35 (29) (2019) 9611–9621.

[6] A. Cihan, T. K. Tokunaga, J. T. Birkholzer, Diffusion-to-imbibition transition in water sorption in nanoporous media: Theoretical studies, Water Resources Research 57 (6) (2021) e2021WR029720.

[7] B. R. Lawn, D. H. Roach, R. M. Thomson, Thresholds and reversibility in brittle cracks: an atomistic surface force model, Journal of materials science 22 (11) (1987) 4036–4050.

[8] K.-T. Wan, N. Aimard, S. Lathabai, R. G. Horn, B. R. Lawn, Interfacial energy states of moisture-exposed cracks in mica, Journal of Materials Research 5 (1) (1990) 172–182.

[9] R. Tait, P. Fry, G. Garrett, Review and evaluation of the double-torsion technique for fracture toughness and fatigue testing of brittle materials, Experimental Mechanics 27 (1) (1987) 14–22.

[10] A. Shyam, E. Lara-Curzio, The double-torsion testing technique for determination of fracture toughness and slow crack growth behavior of materials: a review, Journal of materials science 41 (13) (2006) 4093–4104.

[11] G. Trantina, Stress analysis of the double-torsion specimen, Journal of the American Ceramic Society 60 (7-8) (1977) 338–341.

[12] M. Ciccotti, G. Gonzato, F. Mulargia, The double torsion loading configuration for fracture propagation: an improved methodology for the load-relaxation at constant displacement, International Journal of Rock Mechanics and Mining Sciences 37 (7) (2000) 1103–1113.

[13] M. Madjoubi, M. Hamidouche, N. Bouaouadja, J. Chevalier, G. Fantozzi, Experimental evaluation of the double torsion analysis on soda-lime glass, Journal of materials science 42 (18) (2007) 7872–7881.

[14] J. A. Salem, M. Radovic, E. Lara-Curzio, G. Nelson, Fracture toughness of thin plates by the double-torsion test method, in: 30th International Conference and Exposition on Advanced Ceramics and Composites, no. ICACC-S1-070-2006, 2006, pp. 63–73.

[15] S. Freiman, D. Mulville, P. W. Mast, Crack propagation studies in brittle materials, Journal of Materials Science 8 (11) (1973) 1527–1533.

[16] A. Evans, A method for evaluating the time-dependent failure characteristics of brittle materials—and its application to polycrystalline alumina, Journal of Materials Science 7 (10) (1972) 1137–1146.

[17] J. Pollet, S. Burns, Thermally activated crack propagation—theory, International Journal of Fracture 13 (5) (1977) 667–679.

[18] S. Wiederhorn, Influence of water vapor on crack propagation in soda-lime glass, Journal of the American Ceramic Society 50 (8) (1967) 407–414.

[19] J. Outwater, D. Jerry, On the fracture energy of glass nrl interim genet report, Contract No. NR 3219 (01) (1966).

[20] M. Eskandari-Ghadi, S. Nakagawa, H. Deng, S. Pride, B. Gilbert, Y. Zhang, Surface force and reactant transport controls subcritical crack growth in brittle solids: A theoretical study, Journal of Mechanics Physics of Solids (in review).

[21] J. A. Nelder, R. Mead, A simplex method for function minimization, The computer journal 7 (4) (1965) 308–313.

[22] P. Borcherds, Numerical recipes in c++: The art of scientific computing (2nd edn). numerical recipes example book (c++)(2nd edn). numerical

recipes multi-language code cd rom with linux or unix single-screen license revised version, European Journal of Physics 24 (3) (2003) 329–330.

Graphical Abstract

Inversion-based correction of Double-Torsion (DT) subcritical crack growth tests for crack profile geometry

Seiji Nakagawa, Yida Zhang, Mehdi Eskandari-Ghadi, Donald W. Vasco

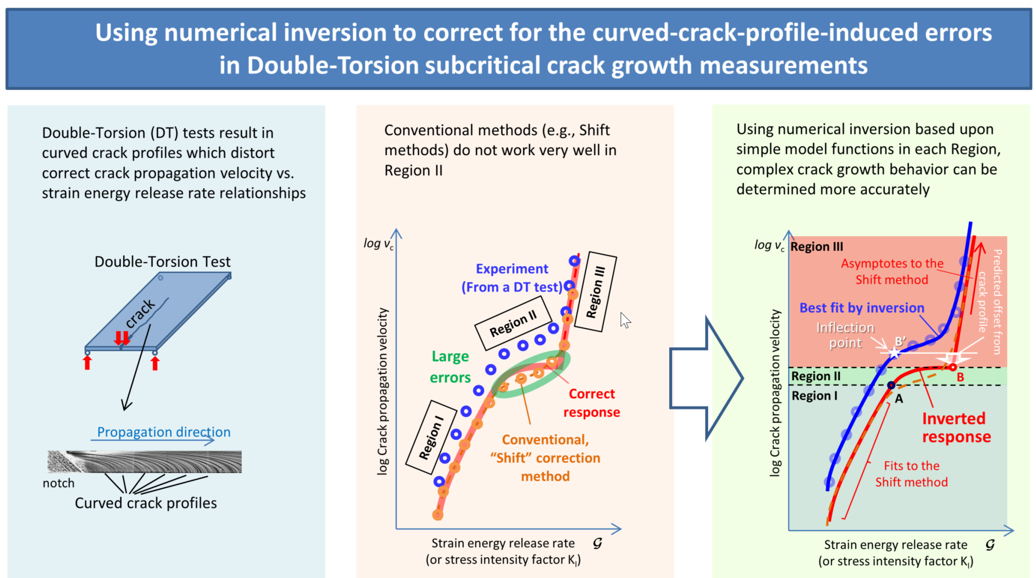

Highlights

Inversion-based correction of Double-Torsion (DT) subcritical crack growth tests for crack profile geometry

Seiji Nakagawa, Yida Zhang, Mehdi Eskandari-Ghadi, Donald W. Vasco

- Double-Torsion tests result in errors in crack speed vs energy release relationship
- Curved and tilted crack front profile causes overestimation of the crack speed
- A new error correction method based upon numerical inversion is developed
- The inversion employs a parameterized models in each crack propagation regime
- Crack behavior in Regions II and III is determined more accurately